

Design and Simulation of TiN-Based Suspended Meander Kinetic Inductance Detectors (KIDs) for Visible and Near-Infrared Astronomy Applications

Maria Appavou ^{1*}, Lucas Ribeiro ^{2†}, Paul Nicaise ^{1†}, Jie Hu ^{1†},
Jean-Marc Martin ^{3†}, Josiane Firminy ^{1†}, Christine Chaumont ^{1†},
Piercarlo Bonifacio ^{4†}, Faouzi Boussaha ^{1†}

^{1*}GEPI, Observatoire de Paris, Université PSL, CNRS, 77 Avenue
Denfert-Rochereau, Paris, 75014, France.

²Université d'Evry Val d'Essonne, 23 Boulevard François Mitterrand,
Evry-Courcouronnes, 91000, France.

³California Institute of Technology, 1200 E. California Blvd., Pasadena,
91125, California, USA.

^{4*}GEPI, Observatoire de Paris, Université PSL, CNRS, 5 Place Jules
Janssen, Meudon, 92195, France.

*Corresponding author(s). E-mail(s): maria.appavou@obspm.fr;
Contributing authors: lucasrib@hotmail.fr; paul.nicaise@obspm.fr;
jie.hu@obspm.fr; jeanmarc@caltech.edu; josiane.firminy@obspm.fr;
christine.chaumont@obspm.fr; piercarlo.bonifacio@obspm.fr;
faouzi.boussaha@obspm.fr;

†These authors contributed equally to this work.

Abstract

We report on simulations of a novel design of optical titanium nitride (TiN)-based Kinetic Inductance Detectors (KIDs) in order to improve their response to optical photons. We propose to separate the meander from the substrate to trap hot phonons generated by optical photons, preventing their rapid propagation through the substrate. These phonons would in turn contribute to the breaking of more Cooper pairs, thereby increasing the response of the detector. In our design, the meander is suspended a few hundred nanometers above the substrate. Furthermore, reflective gold (Au) or aluminum (Al)-based layers can be placed under the meander to improve photon coupling in the optical wavelengths.

Keywords: KID, Suspended Meander, TiNx, Superconductor, Optical and Near-Infrared

1 Introduction

Kinetic Inductance Detectors (KIDs) through their low noise, high readout speed, and large-scale multiplexing are cutting-edge sensors and competitive with other cryogenic detectors such as Superconducting Tunnel Junctions (STJs) and Transition Edge Sensors (TESs) for submillimeter/THz to UV ranges [1]. However, the optimal operation of optical KIDs in spectroscopy is currently hampered by low-measured spectral resolutions. These remain much lower than those predicted by theory given by $R \approx 1/2.355\sqrt{(\eta h\nu/F\Delta)}$ [2, 3], where η is the conversion efficiency of quasiparticles, which is typically of the order of 0.57, $h\nu$ is the photon energy, F is the Fano factor, generally ~ 0.2 , and $\Delta \approx 1.76k_B T_c$ is the energy gap of the superconductor. T_c is its critical temperature and k_B is the Boltzmann constant. The cause of this difference is still not well understood, but studies currently being carried out indicate that it would be due to various sources of noise, whether generated by the readout electronics or by two-level system (TLS) noise featured on the interface between the dielectrics and the superconductor [4], which also reduces the response to optical photons [5, 6].

As R is signal-to-noise ratio-dependent [6], in order to improve the energy-resolving power, one can either decrease the noise or increase the signal response, or both. When it is difficult to further mitigate TLS noise effects, the signal-to-noise ratio, and thus R , can be improved by increasing the signal response. Photon absorption induces a down-conversion cascade involving electron-phonon interaction and hot phonons, which have a higher energy than the Debye energy, will rapidly escape from the superconducting thin film to the substrate and significantly limit the energy-resolving power [7]. A few solutions were explored by other research groups such as the addition of a superconducting thin layer featuring a lower Debye energy [3], between the meander and the substrate, or suspending the meander on a thin membrane [2] in order both to trap phonons within the meander to enhance the Cooper pairs breaking. In this study, we propose to go one step further with the membrane solution and fully suspend the meander, without using a membrane, to further enhance the trapping of hot phonons and increase the response. This design would also allow us to place a reflector under the suspended meander to improve the optical coupling and increase the quantum efficiency (QE). Here, we assume that photons that are not absorbed by the TiN-based meander can pass through before being reflected by the reflector towards the latter.

2 Design

Using SONNET software [8], our simulations are carried out with a sapphire (Al_2O_3) substrate whose relative dielectric constant $\epsilon_{r,\text{Al}_2\text{O}_3}$ is fixed at 9.9. Due to its large 10 eV energy gap, the sapphire is transparent at optical wavelengths, which means that, compared to silicon, the response of the substrate at these wavelengths is considerably

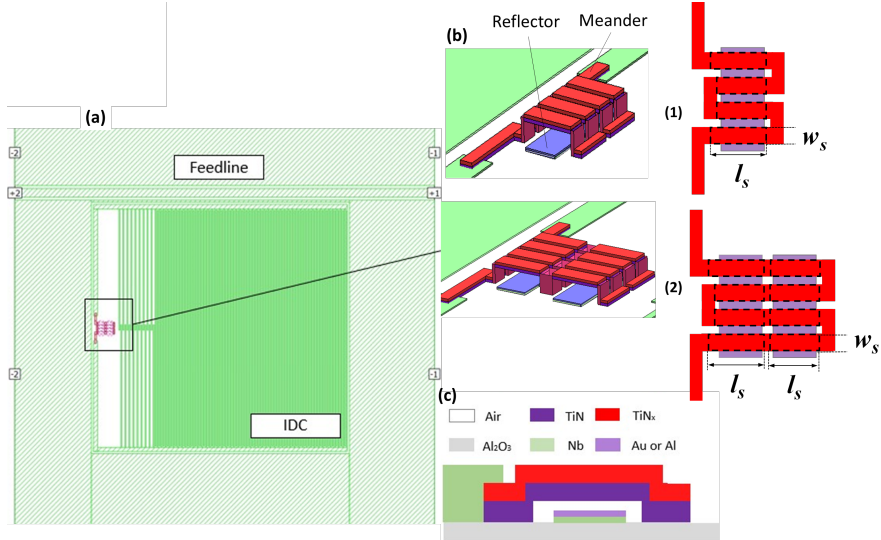


Fig. 1: (a) Top view of a suspended meander KID with a $300 \times 300 \mu\text{m}^2$ interdigitated capacitor (IDC) and a $22 \times 14 \mu\text{m}^2$ meandered inductor. (b) Perspective (right) and top (left) views of the meander along with a reflector (1). For meanders with long strips, they can be divided into shorter sections (two here) which are easier to suspend (2). The dashed lines on top views indicate the suspended areas. (c) Side view of the suspended meander with reflector and the associated materials. For clarity, thicknesses are not to scale.

reduced. As illustrated in Fig. 1, one pixel consists of an interdigitated capacitor (IDC) with a dimension of $300 \times 300 \mu\text{m}^2$ with $1 \mu\text{m}$ wide fingers and $1 \mu\text{m}$ gaps.

Almost the entire meander can be suspended above a single rectangular reflector (Fig. 1-b1), where only the edges are maintained in contact with the substrate. These contact points act as anchor points. The reflector can also be divided into smaller rectangles (Fig. 1-b2) which allows shorter sections to be suspended if it proves difficult to do so with long strips. In this case, the meander will also be in contact with the substrate between the reflectors. It is obvious that contact areas must be as small as possible.

In this study, we consider the configuration with the split reflector (Fig. 1-b2). The meandered inductor has a total dimension of $l_m \times w_m = 22 \times 14 \mu\text{m}$ and $1 \mu\text{m}$ gaps. The resonator is capacitively coupled to a 50Ω coplanar waveguide (CPW) feedline with a $10 \mu\text{m}$ width conducting line separated by $3.5 \mu\text{m}$ width from both ground planes.

The meander consists of a sub-stoichiometric $\sim 1 \text{ K TiN}_x$ thin film and both the IDC and feedline are made of a single niobium (Nb) thin film. Nb has a lower surface impedance making it easier to build the 50Ω feedline. On the other hand, its higher energy gap than that of TiN prevents the diffusion of quasiparticles out of the TiN-based meander where they are generated. The diffusion of quasiparticles out of the absorber can induce pulse height variations [2]. A thin layer of stoichiometric $\sim 4 \text{ K}$

Table 1: Thickness, kinetic inductance, critical temperature, electrical resistivity of the different layers of the absorber and reflector.

Layer (Role)	t [nm]	L_k [pH/ \square]	T_c [K]	ρ_{elec} [$\mu\Omega \cdot \text{cm}$]
Nb ⁵	40	0.2	9.2	15
Au [9] or Al [10] (Reflector) ⁶	30	-	-	0.022 or 0.0001
Vacuum	100-250	-	-	-
TiN (Absorber) ⁵	20	36	4.6	270
TiN _x (Absorber) ⁵	50-150	22-66	0.85	231

⁵ On SONNET, the kinetic inductance is defined as $L_k = \hbar\rho_n/\pi\Delta t$.

⁶ Simulated as normal metals with electrical resistivity ρ_{elec} at $T \approx 1$ K.

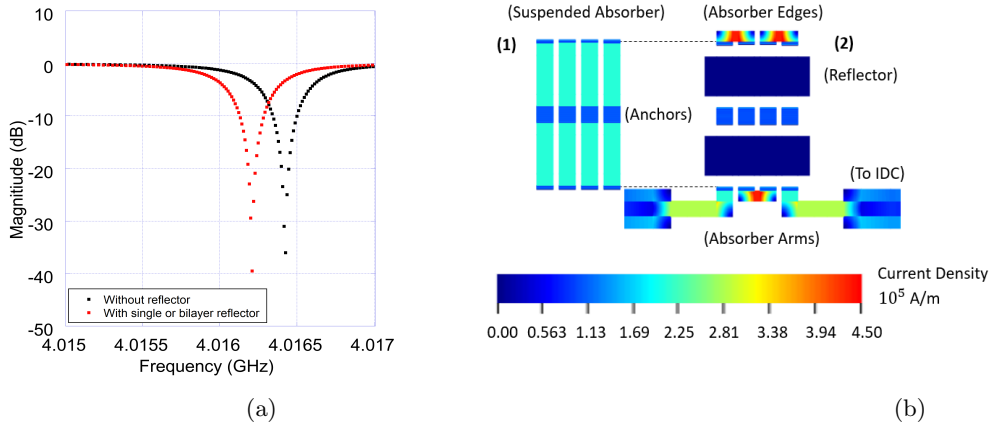


Fig. 2: (a) Frequency-domain representation of the transmission parameter S_{21} for different configurations with vacuum gap (single and bilayer reflector configurations responses overlap). (b) Top view of the meander part showing the distribution of the current density in the suspended meander. (1) shows the suspended meander strips with a current density above 10^5 A/m and (2) close to 0 A/m in the reflector.

TiN is added under the TiN_x layer to reduce the TLS noise by preventing oxidation when suspended. Furthermore, as the measured T_c of the TiN_x layer which meets the optimal mechanical stress parameters to achieve suspended superconducting structures [11] is around 0.8 K, the addition of the TiN allows the overall increase of the meander T_c up to ~ 2 K. In fact, no resonance or very shallow resonances (< 2 dB) were observed with our KIDs made from TiN_x with a low T_c (< 1 K), probably due to high resistive losses. According to our first fabrication process optimizations to assess the best suspension conditions, we found that the meanders can easily collapse for strips of thickness less than 100 nm and length longer than 12 μm . In this case, the length and the thickness of the meander strip to be suspended are set at $l_s = 8 \mu\text{m}$

and $t_{meander} = 120$ nm, respectively. The latter consists of 100 nm of TiN_x and 20 nm of TiN, corresponding to respectively $L_{k,\text{TiN}_x} = 33$ pH/ \square and $L_{k,\text{TiN}} = 36$ pH/ \square . Furthermore, the main parameters of the meander are stated in Tab. 1 as a baseline of the preliminary simulations. Also according to experimental investigations, the addition of a thin 20 nm-thick TiN layer does not alter the stress parameters of the TiN_x layer required to be suspended. The strip width is set at $w_s = 2.7$ μm . Each strip is thus suspended over 2×8 μm -length. The contact area between the superconductor and the substrate is limited to 1.75×2.7 μm^2 per strip at edges and 2.25×2.7 μm^2 per strip at the center. Our fabrication process will be published somewhere else.

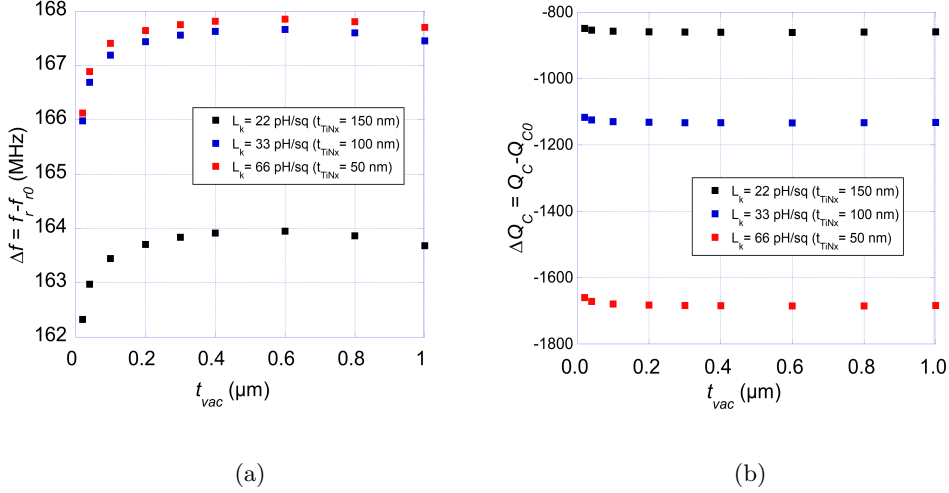


Fig. 3: (a) Resonance frequency Δf_r and (b) coupling quality factor ΔQ_c shifts as a function of the vacuum gap and absorber thickness. Simulated with Nb/Au reflector, $f_{r0} \approx [4.13, 3.85, 3.47]$ GHz and $Q_{c0} \approx [8000, 10000, 13000]$ computed from the unsuspended configuration for respectively $L_k \approx [22, 33, 66]$ pH/ \square .

The addition of reflectors made of gold (Au) or aluminum (Al) beneath the suspended meander would improve the optical coupling by reflecting back the transmitted optical photons [12]. The gap between the meander and the reflector must satisfy the quarter-wave condition for optimal optical coupling $t_{vac} = \lambda/4n$ with $n = 1$. Thus, between $\lambda = 400$ and 1000 nm, the optimal vacuum gap varies between $t_{vac} = 100$ and 250 nm. This vacuum gap range is probably still achievable using the fabrication process implemented to build vacuum capacitor [11]. Finally, a Nb layer is added below the Al or Au reflective layer to minimize the electrical loss with the superconducting proximity effect. To maximize this effect, the thickness of the Nb layer t_{Nb} must be no less than its coherence length $\zeta_{Nb} \approx 40$ nm [13].

3 Simulation Results

We simulate different KID configurations, with and without a suspended meander, to investigate the frequency operation. Each layer of the reflector is progressively added to study their effects on the resonant frequency f_r and coupling quality factor Q_c . This study stresses on Q_c as the total quality factor $1/Q = 1/Q_i + 1/Q_c$. For $Q_c \ll Q_i$, the total quality factor Q can be approximated as $Q \approx Q_c$. The unsuspended meander-based KID (taken as a reference) resonates at $f_{r0} = 3.85$ GHz with a coupling quality factor of $Q_{c0} \approx 10000$. Once the meander is suspended with a vacuum gap of 200 nm, the resonant frequency shifts to higher frequencies with $\Delta f_r = f_r - f_{r0} \approx +168$ MHz (Fig. 2a) and the coupling quality factor slightly decreases $\Delta Q_c = Q_c - Q_{c0} \approx -1000$. This is obviously due to the vacuum gap which reduces the overall parasitic capacitance $C_p \propto \epsilon_{eff}$ within the meander as well as the meander/substrate interface as $\epsilon_{r,vac} = 1 \leq \epsilon_{eff} \leq \epsilon_{r,Al_2O_3}$. Albeit modest, this will probably reduce TLS noise generated by these parasitic capacitances. By adding a single (Au or Al) or bilayer (Nb/Au or Nb/Al) reflector, the frequency shifts towards lower frequencies (Fig. 2a) of only 0.2 MHz ($\Delta f_r \approx +168$ MHz). The coupling quality factor remains around $\Delta Q_c \approx -1000$.

Here, the vacuum gap between the reflector and the meander is also set at 200 nm. This shift in frequency highlights the characteristic behavior of a parasitic capacitance generated this time by the stack made of a reflector, vacuum, and meander which form a metal/vacuum/metal plate capacitor. However, as shown in Fig. 2a, compared with the reference (i.e. the unsuspended meander), the resultant parasitic capacitors produce an overall shift towards higher frequencies indicating that the stack features a weak parasitic capacitor. Unlike reflector-based KIDs which use dielectrics [12], this will probably not introduce additional TLS noises. Furthermore, the contribution of each layer is not differentiated regardless of the number of reflector layers, or metal type as the parasitic capacitance is made of vacuum with a lower dielectric constant $\epsilon_{r,vac} = 1 \leq \epsilon_{r,Al_2O_3} = 9.9$ (Fig. 2a).

Besides, a uniform current density is required to achieve a uniform phase response to incoming photons only within the meander. Fig. 2b shows that it is well uniform in the suspended strips compared to the reflector. Furthermore, to assess the effect of meander suspension with a Nb/Au reflector, we carried out simulations for different vacuum gaps and meander thicknesses. As shown in Fig. 3a, 3b, as expected, for small gaps up to 200 nm where parasitic capacitors are more important, there is a stronger dependency of Δf_r and, to a lesser extent, ΔQ_c on the vacuum gap, whereas, from 200 nm, they remain almost constant. These aspects will be taken into account especially when designing large-scale arrays with a resonance frequency step of 2-4 MHz between each resonance [14].

As reported in [15], only a fraction of the light is absorbed by the meander. The other fraction is either transmitted or reflected. To achieve optimum detector response, the kinetic inductance of the meander should be high and its volume should be small [6]. On top of this, the film absorption should ideally be total. However, for thin TiN layers of a few tens of nm such as those shown in Fig. 4, transmittance becomes non-negligible. The suspended meander design would make it possible to recover the transmitted photons that have passed through the meander to be reflected back towards it thanks to a reflector placed at $\lambda/4$. The effectiveness of this concept

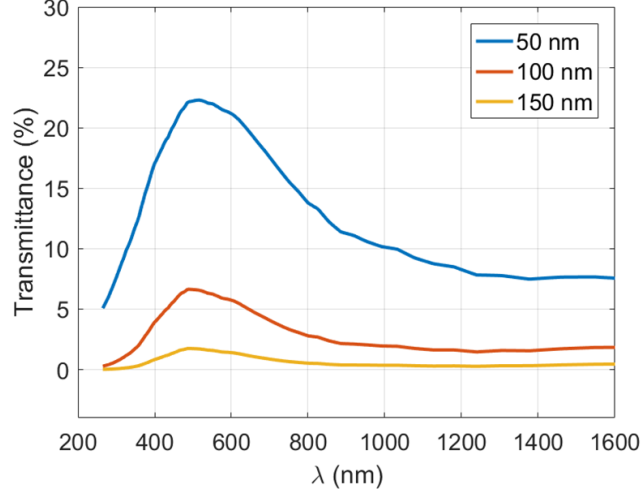


Fig. 4: Simulated transmittance of a single TiN layer for three different TiN thicknesses.

will therefore depend considerably on below the transmission of TiN. Fig. 4 shows the simulated transmittance, obtained by modeling the layer as a transmission line and retrieving the transmission parameter [13], for a single TiN layer for 50, 100 and 150 nm-thick. We notice that the transmittance decreases considerably with the TiN thickness. It decreases by around 70% when the thickness increases from 50 to 100 nm and by around 90% at 150 nm. This prompts the use of the thinnest TiN thickness which will be determined mainly by fabrication constraints.

4 Conclusion and Further Work

By simulation, we have demonstrated the feasibility of an optical suspended meander-based KID design in order to improve response by trapping hot phonons. A superconducting reflector is also placed under the suspended meander at a distance of a quarter wavelength ($\lambda/4$) to improve optical coupling. Compared to the unsuspended configuration, the suspended meander design affects both the resonance frequency and coupling quality factor. The fabrication of suspended meanders is obviously very challenging, especially for thin TiN layer, between 50 and 100 nm-thick, required to improve optical coupling using the reflective layer. This will be done using the process implemented for vacuum capacitor-based KIDs [11]. In parallel, we will also focus on the modeling of the whole meander/vacuum/reflective layer structure using the model of [12].

References

- [1] Ulbricht, G., Lucia, M.D., Baldwin, E.: Applications for Microwave Kinetic Induction Detectors in Advanced Instrumentation. *Applied Sciences* **11**(6), 2671 (2021) <https://doi.org/10.3390/app11062671>
- [2] Visser, P.J., Rooij, S.A.H., Murugesan, V., Thoen, D.J., Baselmans, J.J.A.: Phonon-Trapping-Enhanced Energy Resolution in Superconducting Single-Photon Detectors. *Phys. Rev. Appl.* **16**, 034051 (2021) <https://doi.org/10.1103/PhysRevApplied.16.034051>
- [3] Zobrist, N., Clay, W.H., Coiffard, G., Daal, M., Swimmer, N., Day, P., Mazin, B.A.: Membraneless Phonon Trapping and Resolution Enhancement in Optical Microwave Kinetic Inductance Detectors. *Phys. Rev. Lett.* **129**, 017701 (2022) <https://doi.org/10.1103/PhysRevLett.129.017701>
- [4] Gao, J., Daal, M., Vayonakis, A., Kumar, S., Zmuidzinas, J., Sadoulet, B., Mazin, B.A., Day, P.K., Leduc, H.G.: Experimental evidence for a surface distribution of two-level systems in superconducting lithographed microwave resonators. *Applied Physics Letters* **92**(15) (2008) <https://doi.org/10.1063/1.2906373>
- [5] Hu, J., Boussaha, F., Martin, J.-M., Nicaise, P., Chaumont, C., Beldi, S., Piat, M., Bonifacio, P.: Large inverse transient phase response of titanium-nitride-based microwave kinetic inductance detectors. *Applied Physics Letters* **119**(21) (2021) <https://doi.org/10.1063/5.0074103>
- [6] Boussaha, F., Hu, J., Nicaise, P., Martin, J.-M., Chaumont, C., Dung, P.V., Firminy, J., Reix, F., Bonifacio, P., Piat, M., Geoffray, H.: Photon-counting with single stoichiometric TiN layer-based optical MKIDs. *Applied Physics Letters* **122**(21), 212602 (2023) <https://doi.org/10.1063/5.0147584>
- [7] Kozorezov, A.G., Wigmore, J.K., Martin, D., Verhoeve, P., Peacock, A.: Electron energy down-conversion in thin superconducting films. *Phys. Rev. B* **75**, 094513 (2007) <https://doi.org/10.1103/PhysRevB.75.094513>
- [8] Sonnet 3D Planar High-Frequency Electromagnetic Software. <https://www.sonnetsoftware.com/>
- [9] Matula, R.A.: Electrical resistivity of copper, gold, palladium, and silver. *Journal of Physical and Chemical Reference Data* **8**(4), 1147–1298 (1979) <https://doi.org/10.1063/1.555614>
- [10] Desai, P.D., James, H.M., Ho, C.Y.: Electrical Resistivity of Aluminum and Manganese. *Journal of Physical and Chemical Reference Data* **13**(4), 1131–1172 (1984) <https://doi.org/10.1063/1.555725>

- [11] Boussaha, F., Beldi, S., Monfardini, A., Hu, J., Calvo, M., Chaumont, C., Levy-Bertrand, F., Vacelet, T., Traini, A., Firminy, J., Piat, M., Reix, F.: Development of TiN Vacuum-Gap Capacitor Lumped-Element Kinetic Inductance Detectors. *Journal of Low Temperature Physics* **199**(3–4), 994–1003 (2020) <https://doi.org/10.1007/s10909-019-02309-0>
- [12] Nicaise, P., Hu, J., Martin, J.-M., Beldi, S., Chaumont, C., Bonifacio, P., Piat, M., Geoffray, H., Boussaha, F.: Investigation of Optical Coupling in Microwave Kinetic Inductance Detectors Using Superconducting Reflective Plates. *Journal of Low Temperature Physics* **209**(5-6), 1242–1248 (2022) <https://doi.org/10.1007/s10909-022-02789-7>
- [13] Nicaise, P.: Development of Microwave Kinetic Inductance Detectors for Visible and Near-IR Astronomy Applications. PhD thesis (2022). <https://theses.hal.science/tel-04021231>
- [14] Hu, Jie and Nicaise, Paul and Boussaha, Faouzi and Martin, Jean-Marc and Chaumont, Christine and Marret, Alexine and Reix, Florent and Firminy, Josiane and Vacelet, Thibaut and Pham, Dung and Piat, Michel and Caffau, Elisabetta and Bonifacio, Piercarlo: Development of MKIDs in the Optical and Near-Infrared Bands for SPIAKID. *Journal of Low Temperature Physics*, 1–12 (2023) <https://doi.org/10.1007/s10909-023-03018-5>
- [15] P. Szypryt and B. A. Mazin and G. Ulbricht and B. Bumble and S. R. Meeker and C. Bockstiegel and A. B. Walter: High quality factor platinum silicide microwave kinetic inductance detectors. *Applied Physics Letters* **109** (2016) <https://doi.org/10.1063/1.4964665>